7-1-2005

# Expandable Graphite/Polyamide-6 Nanocomposites

Fawn Marie Uhl
*Marquette University*

Qiang Yao
*Marquette University*

Hiroyoshi Nakajima
*Pennsylvania State University - Main Campus*

Evangelos Manias
*Pennsylvania State University - Main Campus*

Charles A. Wilkie
*Marquette University*, charles.wilkie@marquette.edu

Accepted version. *Polymer Degradation and Stability*, Vol. 89, No. 1 (July 2005): 70-84. DOI. 

*Polymer Degradation and Stability*, Vol. 89, No. 1 (July 2005): 70-84. DOI. 

# Expandable Graphite/Polyamide-6 Nanocomposites

Fawn M. Uhl
Department of Chemistry, Marquette University, Milwaukee, WI
Qiang Yao
Department of Chemistry, Marquette University, Milwaukee, WI
Department of Chemical Engineering, Polytechnic University, Six Metrotech Center, Brooklyn, NY
Hiroyoshi Nakajima
Department of Materials Science and Engineering, Penn State University, University Park, PA
E. Manias
Department of Materials Science and Engineering, Penn State University, University Park, PA
Charles A. Wilkie
Department of Chemistry, Marquette University, Milwaukee, WI

## Abstract

Polyamide-6 (PA-6)/graphite nanocomposites were prepared by melt blending, using a variety of graphites, including virgin graphite, expandable graphites and expanded graphite. The resulting nanocomposites were characterized by X-ray diffraction, thermogravimetric analysis, cone calorimetry, and tensile mechanical analysis. Nanocomposite formation does occur, as denoted by the nanometre dispersion of graphite layers in the polymer matrix, and the dispersion depends on the graphite treatment. The material properties of the resulting

composites are improved relative to the virgin/unfilled polymer; in particular, there is an enhancement of the thermal stability without any significant deterioration of the mechanical properties.


## Keywords

Expandable graphite, Polyamide-6, Nanocomposites


## 1. Introduction

Polymer nanocomposites are attracting a great deal of attention and have been the focus of study for a large number of research groups. In particular, polymer/layered-inorganic and polymer/clay nanocomposites are being explored extensively due to their high promise for potential applications [1], [2], [3] and as model systems for nanoscopically confined polymers [4], [5]. These polymer/inorganicnanocomposites can be prepared by in situ polymerisation, including solution, suspension, emulsion, and bulk polymerisations, as well as by melt blending and solution mixing [6], [7], [8], [9], [10], [11], [12], [13]. Polymer/clay nanocomposites consist of nanometre-thin clay layers dispersed in a polymer matrixand they exhibit an unusually broad range of properties that are concurrently improved [1], [2], [3], such as mechanical, thermo-mechanical, barrier, and flame retardancy [14], [15], [16], [17], while maintaining the light-weight character and the optical clarity of the polymer [18]. Since the pristine clays are only miscible with hydrophilic polymers [19], [20], for the vast majority of polymer matrices it is necessary that appropriate surfactants are employed in order to promote interactions that are favourable for mixing between clay and polymer [21], [22]. Depending on the polymer/clay miscibility, nanocomposites can be divided into three idealized types: “immiscible nanocomposites” in which the nano-fillers are not dispersed and agglomerate in micrometer-size stacks which behave as the effective inorganic fillers (cf. microcomposites or conventional composites); “intercalated nanocomposites” in which nanometre-thin polymer films are inserted in-between the individual clay platelets, while maintaining the parallel-stacked clay registry; and “exfoliated nanocomposites” in which the nanometre-thin clay layers are dispersed throughout the polymer matrix homogeneously with no marked memory of their previous parallel registry (cf. delaminated nanocomposites).

One of the most impressive nanocomposites prepared to date is the polyamide-6 (PA-6)/montmorillonite-clay nanocomposites. These hybrids have been prepared by melt blending and by in situ polymerisation, yielding an exfoliated structure independent of the composite formation route [16], [23], and exhibiting impressive improvements for a wide range of properties [1]. PA-6/montmorillonite nanocomposites show an excellent improvement over PA-6 in mechanical properties and especially in heat distortion temperature (HDT) [1], [14]. At the same time, the thermal stability of PA-6 nanocomposites is similar to that of pure PA-6, while the peak heat release rate, as measured by cone calorimetry, is decreased by approximately 60% [14], accompanied by a reduction in the mass loss rate. Today, it is well established that the clay fillers promote the γ crystalline phase in the PA-6 composites mediated by strong hydrogen bonding of the amide groups to the silicate surfaces of the clay, whereas the neat PA-6 predominately exhibits the α phase [16], [24], [25]. A number of the property enhancements – specifically the impressive increase in the HDT and improvement of the mechanical properties – are currently attributed to this clay-induced γ crystalline phase [24], [25], however other effects – in particular the flammability behaviour – are suggested to originate from the composite structure [14] (i.e. the dispersion of the nanometre-thin layered fillers). Inspired by the behaviour of these systems, and in order to better understand the structure–property relations in these nanocomposites systems, we herein undertake a study of the same polymer (PA-6) and the nanometre-thin layered filler (graphite) that has a similar geometry with the montmorillonite clays but does not offer hydrogen bonding sites for the polyamide.

Graphite is a layered material, consisting of a structure where carbon atoms are bound by covalent bonds to other carbons in the same plane and only van der Waals forces are acting between successive layers. Since the van der Waals forces are relatively weak, it is possible for a wide range of atoms, molecules, and ions to intercalate between graphite sheets [26], [27], [28], [29], [30]. In contrast to the clays, there is no net charge on graphite; thus, ion exchange processes like those used to organically modify clays, are not possible for graphite. However, graphite intercalation compounds, also known as *expanded graphite*, may provide a possible source

for nanocomposite formation with polymers. For instance, compounds of potassium and graphite, $KC_8$ and $KC_{24}$, that have been used as a catalyst for many years for the preparation of polymers [31], [32], [33], [34], (the graphite is typically removed by filtration after preparation), have been recently identified to yield structures reminiscent of nanocomposites [35]. Likewise, Pan et al. observed that expanded graphite could be equilibrated with monomer resulting in the graphite sheets being further exfoliated and dispersed within the PA-6 matrix [17]. The mechanical properties of this PA-6/graphite nanocomposites were reduced for loadings above 2% graphite; a behaviour attributed to the reduced mobility of the PA-6 by the graphite sheets, which resulted in a reduced crystallite growth [17]. Another class of graphite compounds that may be utilized to disperse in polymers are materials like the graphite–sulfuric acid system [36], where the intercalation of sulfuric acid can be done chemically or electrochemically [17]. This material is frequently referred to as an *expandable graphite* because upon heating one may drive out the sulfuric acid, typically as reduction products, with an accompanied expansion of the interlayer (i.e. an increase in the *d*-spacing). The *d*-spacing in expandable graphite increases from 0.335 nm to approximately 0.789 nm [37], and upon heating one obtains expanded graphite, in which an increase in the *d*-spacing of several hundreds times along the *c* axis is observed [38]. Expandable graphite can also be used for the preparation of PA-6/graphite nanocomposites by in situ polymerisation [39], [40]. Upon polymerisation the graphite layers were further delaminated and dispersed within the PA-6 matrix, as demonstrated by TEM micrographs. In these systems, the equilibrium melting temperature of PA-6 was reported to decrease with the graphite addition, a behaviour also attributed to the hindrance of the PA-6 chains' motion during crystallization, which resulted in less perfect PA-6 crystals [39]. Although much effort has been paid to the electrical properties of polymer/graphite nanocomposites, there are few reports regarding the effect of graphite on the thermal stability and/or flame retardancy of the polymer [26].

In this study, we attempt a comprehensive study of structure, thermal, mechanical properties, and flame retardancy of PA-6 and PA-6/graphite nanocomposites prepared by melt blending; the emphasis is on how the various treatments of graphite affect the composite structure and the material properties. Parallels are drawn to the much better studied PA-6/montmorillonite-clay nanocomposites, in order to elucidate those effects that originate from the composite structure and distinguish them from those caused by the PA-6/silicate hydrogen bonding.

# 2. Experimental

## 2.1. Materials

Virgin graphite (VG) (1–2 μm) and polyamide-6 (PA-6) were obtained from Aldrich Chemical Company and used as received. Expandable sulfuric acid-intercalated graphite (GIC) and expanded graphite (EG) were obtained from UCAR Graph-Tech Inc. and used as received. The expandable graphites (under the commercial name GRAFGuard) are denoted by: GIC-220B, GIC-220A, GIC-220N, and GIC-160A, where the number (220 or 160) represents the onset temperature for the release of the sulfuric acid, and the letter (A, B, and N) represents the surface treatment of the graphite: acidic, basic, and neutral, respectively. All of the graphites are of 80 mesh particle size. EG is a “milled to dust” expanded graphite (TG406).

## 2.2. Measurements

A Cahn TG-131 thermogravimetric analyser was used under a flowing nitrogen atmosphere at a scan rate of 20 °C/min. All TGA results are the average of at least two runs; typically the temperatures are reproducible to ±5 °C while the fraction of non-volatile material typically has error bars of ±2%. Infrared spectra were obtained using a Nicolet Magna infrared 560 spectrometer E.S.P. TGA/FT-IR were performed on a Cahn TG-131 balance interfaced to a Mattson Research Fourier transform infrared spectrometer under inert atmosphere at a scan rate of 20 °C/min. X-ray diffraction (XRD) was performed on a Rigaku Geiger Flex, 2-circle powder diffractometer using CuKα radiation ($\lambda$ = 1.54 Å); generator tension is 50 kV and generator current is 20 mA. Scans were taken from $2\vartheta$ at 0.70° to 30°, step size 0.10°, and scan time per step of 20 s using the high resolution mode. Cone calorimetry was performed using an Atlas Cone-2 instrument, according ASTM E 1354-92 at an incident flux of 35 kW/m$^2$ using a cone shaped heater. Exhaust flow was set at 24 L/s and the spark was continuous until the

sample ignited. All cone samples were run in duplicate and typical results from cone calorimetry are considered reproducible to ±10% [41]. Mechanical testing was performed on an Instron tensile testing machine at a crosshead speed of 0.2 in./m; the samples were prepared by stamping from a sheet and the reported results are the average of five determinations. Dynamic mechanical properties of the compression-moulded samples were measured by a dynamic mechanical thermal analysissystem (TA Instruments Thermal Analysis Model 2980 – DMA Multifrequency-Tension) in the cantilever mode under nitrogen. The frequency used was 1 Hz and the heating rate was 5 °C/min. Bright field transmission electron microscopy (TEM) images of PA-6/graphite nanocomposite were obtained with a JEOL 1200 IIEX operated with an accelerating voltage of 80 kV, and equipped with a Tietz F224 digital camera. Ultrathin sections (70–100 nm) of the PA-6/graphite nanocomposite were obtained with an ultramicrotome (Leica Ultracut UCT) equipped with a diamond knife. The sections were transferred to carbon-coated copper grids (200 mesh).

### 2.3. Preparation

PA-6/graphite composites were prepared by melt blending at 250 °C for 10 min using a Brabender Plasticorder twin-head mixer. Where annealing was done, it was carried out at 120 °C for 24 h in a vacuum oven, and both annealed and non-annealed samples were characterized.

## 3. Results and discussion

### 3.1. Structure of PA-6/graphite composites

Graphite is a layered material which is characterized by strong intralayer covalent bonds within the carbon layers and weak van der Waals interaction between successive carbon layers. For virgin graphite, the *d*-spacing (the distance between successive carbon layers) is 3.35 Å, or $2\vartheta = 26.6°$ for the XRD apparatus ($\lambda_{CuK\alpha}$) used in this study, as shown in Fig. 1(a). A variety of atoms and molecules can be intercalated between the carbon sheets, resulting in the formation of the intercalated graphite (i.e. expandable graphite) and yielding an increased *d*-spacing (Fig. 1(a)). In Table 1 we tabulate the characteristic *d*-spacings for the expandable graphites (sulfuric acid-intercalated graphites) used in this study. In addition to the original peak of virgin graphite, these systems show additional XRD peaks, which correspond to sulfuric acid-intercalated layers. It is clear from the XRD results (Table 1) that some of these expandable graphites are largely composed of a single intercalated structure (e.g. GIC-200A and GIC-220N), whereas others (namely, GIC-220B and GIC-160A) show the coexistence of non-intercalated and of sulfuric acid-intercalated layers, even though their structures depend on the treatment condition. Expanded graphite shows only the major graphite peak without any additional peaks indicative of intercalation. In Fig. 1(b) the XRD of the polyamide-6 before and after heat treatment (annealing or melt blending) is shown. The PA-6 as received shows two peaks, near $2\vartheta = 20°$ and 25°, while PA-6 that has been melt blended shows an additional third peak, near $2\vartheta = 22°$; this new peak is traditionally associated with the γ crystalline form [16], so melt blending affects conversion of the α form to the γ form of PA-6 even in absence of any filler.

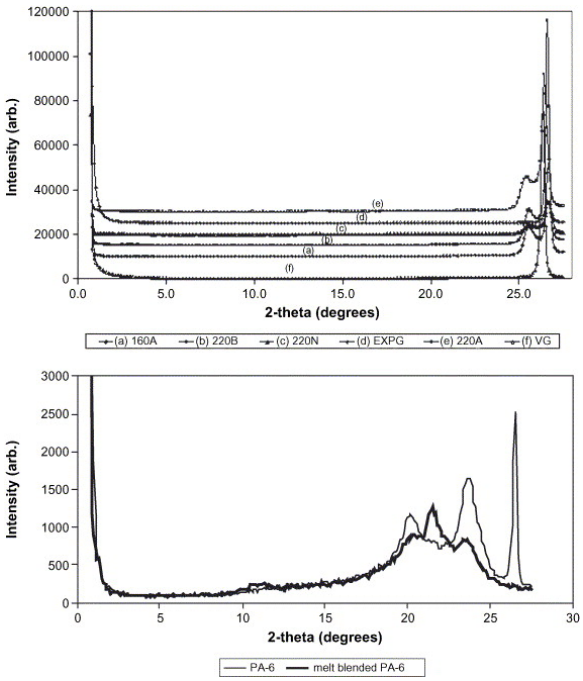


Fig. 1. X-ray diffraction patterns of the two components of the nanocomposite: (a) graphites, and (b) PA-6 before and after heat treatment (annealing or melt blending).

Table 1. XRD results of various graphites

| **Graphites** | **2$\vartheta$ (°)** | ***d*-Spacing (Å)** |
|---|---|---|
| VG[a] | 26.6 | 3.35 |
| GIC-220A[b] | 13.4 | 6.59 |
| GIC-220N[b] | 13.4 | 6.59 |
| GIC-220B[b] | 3.4,13.3 | 6.65, 25.9 |
| GIC-160A[b] | 3.6, 11.8, 13.8 | 6.42, 7.50, 24.5 |
| EG[c] | – | – |

[a]Virgin graphite.
[b]Expandable graphite (sulfuric acid-intercalated graphite).
[c]Expanded graphite.

Upon mixing the graphites with the polymer (PA-6), the structure of the graphites changes, reflecting the extent of dispersion during the nanocomposite formation. XRD patterns and typical TEM images of selected nanocomposites are shown in Fig. 2, Fig. 3, Fig. 4, and for comparison the XRD patterns of the rest of the systems are shown in Fig. 5, Fig. 6, Fig. 7. It is of interest to note the absence of the peak due to the γ-phase of PA-6 after melt blending in the presence of the graphites. Since this peak is always observed upon melt blending of PA-6, its absence must be significant and may indicate that the presence of graphite retards the formation of the γ-phase. For PA-6/GIC-220A, PA-6/GIC-160A and PA-6/GIC-220B, there is no diffraction peak below $2\vartheta = 15°$, even though a peak corresponding to original (virgin) graphite can be observed at $2\vartheta \sim 26°$. Since PA-6 does not show a strong peak at $2\vartheta \sim 26°$, the sharp diffraction peak at $2\vartheta \sim 26°$ in PA-6/graphite nanocomposites should be attributable to the non-expanded (intercalated/exfoliated) graphite. The appearance of this sharp peak suggests that not all of the graphite galleries were expanded and subsequently not all the layers were dispersed in PA-6. Thus, the XRD results indicate that all of PA-6/graphite nanocomposites in this study include some non-dispersed graphite layers, probably originating from non-expanded graphite clusters. The absence of any "intercalated" diffraction peak in the low $2\vartheta$ region is evidence that those layers that were dispersed in PA-6 did not maintain their parallel registry, but rather dispersed in an exfoliated or disordered manner through the polymer matrix.

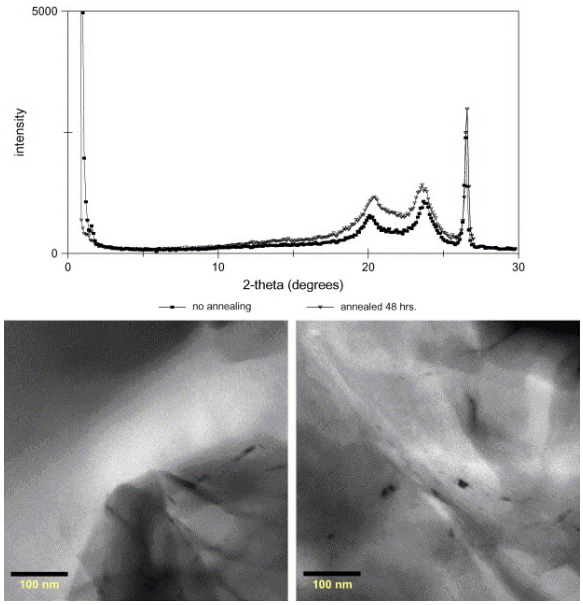

Fig. 2. X-ray diffraction patterns and TEM images for PA-6/VG system at 3% graphite.

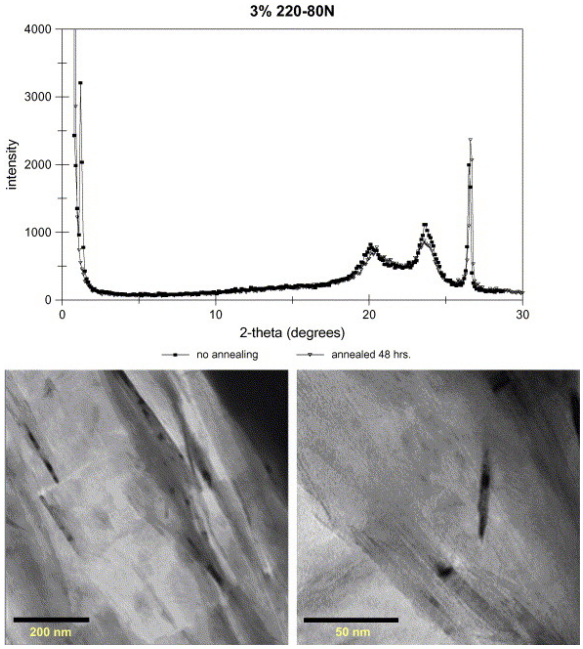

Fig. 3. X-ray diffraction patterns and TEM images of PA-6/GIC-220N at 3% graphite loading.

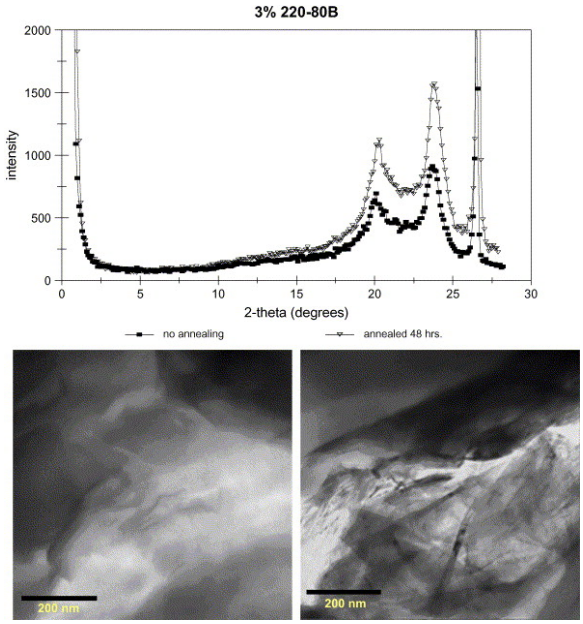

Fig. 4. X-ray diffraction patterns and TEM images for PA-6/GIC-220B at 3% graphite.

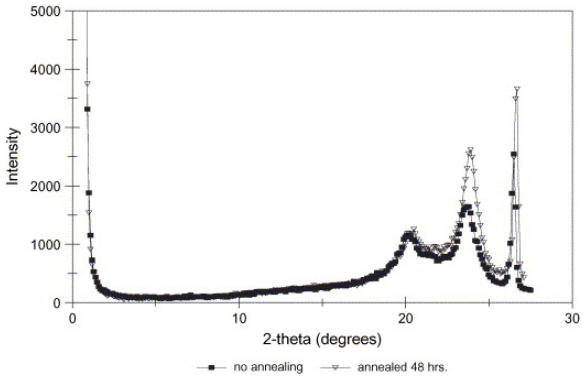

Fig. 5. X-ray diffraction patterns for PA-6/GIC-220A at 3% graphite.

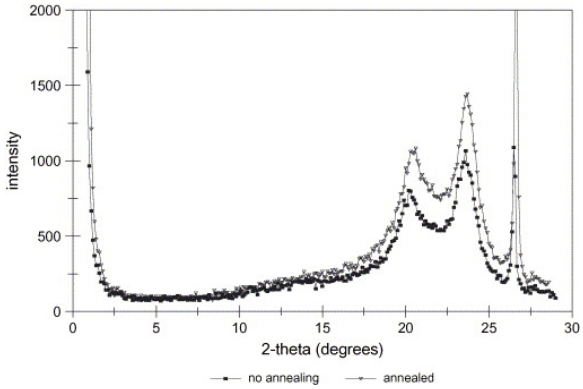

Fig. 6. X-ray diffraction patterns for PA-6/GIC-160A at 3% graphite.

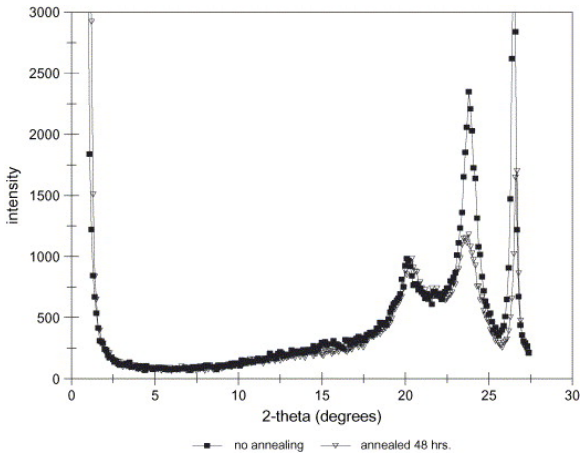

Fig. 7. X-ray diffraction patterns for PA-6/expanded graphite at 3% graphite.

This assumption is supported by the direct observation of the graphites obtained through TEM imaging. In particular, for PA-6/GIC-220B nanocomposites (Fig. 4), well-dispersed graphite layers are observed in all high magnification images. Moreover, there is a coexistence of single dispersed graphite layers and of 'tactoids' consisting of several layers. These results could be indicative of the exfoliated/disordered PA-6/GIC-220B nanocomposite, even though these nanocomposites do not resemble the in situ polyamide-6/clay nanocomposites [1], [23], [24], [25], wherein almost all silicatelayers are exfoliated/disordered throughout the polymer matrix, they do resemble melt-miscible polymer/montmorillonite nanocomposites [6], [18] where a coexistence of fully exfoliated and partially miscible (e.g. intercalated) layers is the norm.

In contrast, the PA-6/VG and PA-6/GIC-220N composites show XRD peaks at $2\vartheta = 1.25°$ and 26.6°, indicating that they do have also intercalated graphite layers. TEM images can provide us more direct information about these structures. For PA-6/GIC-220N (Fig. 3), it is obvious from the TEM that clusters of graphites exist throughout the polymer matrix at a low-magnification. At higher magnification, the individual carbon layers can be clearly seen, in intercalated assemblies as well as in well-dispersed single graphite layers. Furthermore, for the PA-6/VG nanocomposite (Fig. 2), there exist numerous intercalated/immiscible graphite structures (clearly observed at low TEM magnifications) and considerably less exfoliated/disordered graphites, even at higher magnifications. From the combined XRD and TEM results, we can conclude that PA-6/VG and PA-6/GIC-220N nanocomposites have an immiscible/intercalated and intercalated/exfoliated structure, respectively. Since the expandable graphites can be used as intumescent flame retardant agents and the onset expansion temperature of these graphites is 160 °C or 220 °C, the expansion of graphite layers may occur more or less at processing temperature (250 °C).

Finally, a few comments can be made for the effect of heat treatment (annealing) on the crystal structure of PA-6. Annealing of neat (unfilled) PA-6, typically results in an increased density and a preference for the α crystal form [42]. Kojima et al. [43] have shown by DSC measurement of annealed PA-6 under pressure that only one endothermic peak is observed, due to the α form. Also, annealing leads to a decrease in the γ form, since the transition of γ to α form is enhanced by PA-6 hydrogen bonding. Simal and Martin [44], [45] have examined the shrinkage behaviour of PA-6 and PA-6,6. For PA-6 they observed that heat treatment leads to changes in orientations where the generation of nuclei crystallites control the recrystallisation of PA-6. It was found that as annealing temperatures increase the recrystallisation process is favoured, especially at temperatures greater than $T_g$. They have shown that from room temperature to ~120 °C there is a loss in global orientation and have suggested that this may be due to loss of orientation in amorphous region. In contrast to the unfilled PA-6 behaviour, nanocomposites of PA-6 with montmorillonite clay layered fillers strongly promotes the γ crystal phase [24], [25], a behaviour that has been traced to the strong hydrogen bonding of the PA-6 to the silicate-surface oxygens. Despite this very rich phenomenology of heat-treated PA-6, in this work it is apparent from the XRD curves that annealing has no marked effect on the PA-6/graphite nanocomposites. Moreover, in contrast

with PA-6/montmorillonite nanocomposites, due to the absence of any hydrogen bonding between the PA-6 and the graphite fillers, there is no marked enhancement of the γ PA-6 phase.

## 3.2. Flammability behaviour of PA-6/graphite composites

### 3.2.1. Cone calorimetry

To characterize the flame retardancy of polymer composite, cone calorimetry can be used. Previous observations by Gilman et al. [46], showed that although there is no change in the peak heat release rate (PHRR) for an immiscible system, there is a substantial change for both intercalated and exfoliated systems. The reduction in PHRR depends upon the polymer under study but the general rule is that one can expect to see the maximum reduction for nanocomposites and a much smaller reduction, on the order of 10% or less, for immiscible systems [47]. Since the error bars in cone calorimetry are of the order of ±10% [41], this would result in no marked change in the PHRR. The absence of a peak in the XRD patterns could be attributed either to the formation of an exfoliated structure or an immiscible but disordered structure. Cone calorimetry should be able to discriminate between these two situations, since a negligible reduction in PHRR would indicate no nanocomposite formation, while a significant reduction would indicate an exfoliated system.

The cone calorimetry data are shown in Table 2, where the data for peak heat release rate (PHRR), the mass loss rate (MLR), the specific extinction area (SEA), a measure of smoke, are tabulated. The complete cone calorimetry results are displayed graphically in Fig. 8. For those systems that exhibited good dispersions in the XRD and TEM studies, a reduction in PHRR that is comparable to that observed for clay–polymer systems [14] is clearly indicative of nanocomposite formation. For systems that exhibited less miscibility, like the PA-6/VG and PA-6/EG composites, there is essentially no reduction in PHRR, regardless of the graphite loading. For the expandable graphite, there is a small reduction, in the range of 20% at 1% graphite but this increases to 50 and even 60% as the amount of graphite increases. These values are comparable to those obtained by Gilman et al. for PA-6/clay systems [14], [41]. The cone calorimetry results complement very clearly the XRD and TEM results, and in all cases provide a sensitive assessment of the extent of graphite dispersion in the PA-6 matrix. Low reductions in PHRR clearly correlate with disordered/immiscible systems (as for the graphite and expanded graphite cases), whereas well-dispersed systems, i.e., nanocomposites, exhibit substantial reductions in PHRR; a response that correlates well with the absence of an XRD peak.

Table 2. Cone calorimetric data for PA-6/graphite nanocomposites

| Graphite | Graphite loading (%) | PHRR (kW/m$^2$) | Avg. HRR (kW/m$^2$) | Total heat rel. (MJ/m$^2$) | Avg. SEA (m$^2$/kg) | Avg. mass loss (g/s m$^2$) |
|---|---|---|---|---|---|---|
| – | 0 | 1006 ± 55 | 589 ± 9 | 106 ± 9 | 195 ± 12 | 25 ± 1 |
| – | 0[a] | 1053 ± 30 | 592 ± 40 | 111 ± 5 | 205 ± 4 | 24 ± 1 |
| VG | 1 | 967 ± 115 | 557 ± 51 | 98 ± 2 | 186 ± 4 | 23 ± 2 |
| | 3 | 977 ± 30 | 504 ± 68 | 102 ± 5 | 186 ± 5 | 23 ± 2 |
| | 5 | 889 ± 117 | 439 ± 138 | 100 ± 3 | 188 ± 25 | 21 ± 4 |
| EG | 1 | 1005 ± 118 | 532 ± 24 | 107 ± 6 | 182 ± 16 | 23 ± 3 |
| | 3 | 954 ± 153 | 454 ± 178 | 106 ± 11 | 193 ± 13 | 21 ± 2 |
| | 5 | 1042 ± 30 | 524 ± 40 | 105 ± 11 | 181 ± 16 | 22 ± 2 |
| GIC-160A | 1 | 723 ± 132 | 422 ± 54 | 100 ± 1 | 188 ± 26 | 17 ± 2 |
| | 3 | 509 ± 24 | 377 ± 37 | 97 ± 7 | 163 ± 10 | 14 ± 2 |
| | 5 | 454 ± 24 | 305 ± 65 | 93 ± 10 | 225 ± 31 | 13 ± 1 |
| GIC-220A | 1 | 705 ± 74 | 421 ± 25 | 103 ± 7 | 187 ± 8 | 17 ± 1 |
| | 3 | 581 ± 37 | 343 ± 7 | 102 ± 8 | 246 ± 45 | 14 ± 1 |
| | 5 | 472 ± 4 | 306 ± 32 | 93 ± 12 | 218 ± 26 | 13 ± 1 |
| GIC-220B | 1 | 684 ± 29 | 387 ± 42 | 106 ± 6 | 205 ± 10 | 17 ± 1 |
| | 3 | 405 ± 78 | 258 ± 41 | 99 ± 4 | 241 ± 31 | 10 ± 2 |
| | 5 | 364 ± 105 | 229 ± 107 | 93 ± 7 | 162 ± 27 | 10 ± 3 |

| | | | | | | |
|---|---|---|---|---|---|---|
| | 5[a] | 530 ± 17 | 371 ± 13 | 109 ± 5 | 259 ± 12 | 14 ± 1 |
| GIC-220N | 1 | 768 ± 180 | 456 ± 51 | 109 ± 5 | 161 ± 4 | 18 ± 3 |
| | 3 | 565 ± 64 | 324 ± 25 | 104 ± 5 | 234 ± 14 | 14 ± 1 |
| | 5 | 465 ± 28 | 340 ± 15 | 98 ± 1 | 220 ± 62 | 13 ± 1 |

PHRR, peak heat release rate; avg. HRR, average heat release rate; total heat rel., total heat released; avg. SEA, average specific extinction area, a measure of smoke; avg. mass loss, mass loss rate.
[a]Annealed samples.

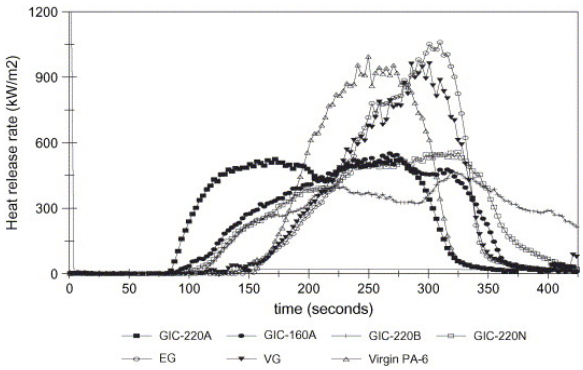


Fig. 8. Heat release rate curves for the various PA-6/graphite nanocomposites at 3% graphite.

In the cases of polymer/clay nanocomposites, including also PA-6/montmorillonite systems, two mechanisms have been suggested to explain the ability of clay to reduce the PHRR: (a) a barrier effect [48] resulting from a high-carbonaceous surface char, and (b) the presence of paramagnetic iron that may cause radical trapping reactions [49]. Radical trapping has been shown to be more important at low amounts of clay, while the barrier properties are more important at higher filler loadings and good dispersions. There is no reason to expect graphite to behave significantly different than the clay layers. With clay, typically 2% inorganic clay is required to form a suitable barrier so the absence of an effect at 1% graphite is not surprising. The evaluation of the smoke that evolves under fire conditions is another property of interest and concern. In general, the smoke that arises from burning a polymer/clay nanocomposite is somewhat larger than what arises from the virgin polymer. The values of the specific extinction area are slightly larger for these graphite nanocomposites, exactly as observed in the clay systems.

Finally, one can also examine the loss of mass for these systems. There is not a significant reduction for PA-6/VG and PA-6/EG composites, but the PA-6/GIC nanocomposites show significant reduction (Fig. 9). The change in PHRR and mass loss rate are in concert with each other and clearly improve when nanocomposite formation occurs, whereas a substantial change is not observed for systems with limited or no graphite exfoliation (microcomposites).

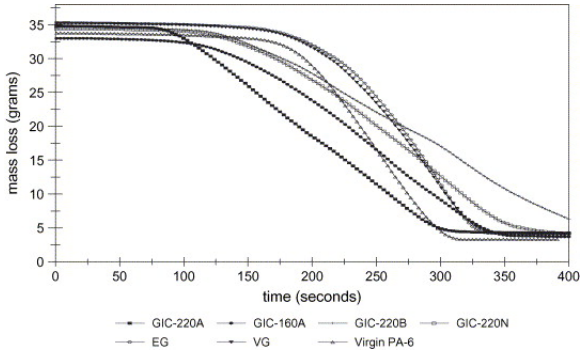


Fig. 9. Mass loss plots for PA-6/graphite nanocomposites at 3% graphite.

It is apparent that the expandable graphite performs much better than the virgin graphite or the expanded graphite. These nanocomposites were formed by melt blending at a temperature above that at which sulfuric

acid is released and it is likely that the explanation for these excellent flammabilityresults arises in some way from the presence of the sulfuric acid, perhaps some intumescent effect, rather than the extent of exfoliation. Further work is underway in an attempt to better understand these effects. The group at DSM has studied the effect of melamine polyphosphate on the degradation of PA-6 and PA-6,6 [50]. They have suggested that this material releases phosphoric acid upon heating and that this phosphoric acid is involved in some way in stabilization of the degrading polymer. A similar process likely occurs for the sulfuric acid graphite system.

### 3.2.2. Thermogravimetric analysis (TGA)

To further explore the thermal decomposition of the various PA-6/graphite composites, thermogravimetric analyses of non-annealed and annealed composites were also undertaken. The TGA data for non-annealed PA-6/graphite nanocomposites (Table 3) show that for the graphite containing no acid (powder, 1–2 μm, and EG) there is no significant difference in onset temperature of degradation, except in case of 1% graphite. However, a significant increase (10–24 °C) in the maximum temperature of degradation is observed, which suggests that the thermal stability of PA-6 is enhanced by the presence of graphite. This is somewhat different for what is observed with PA-6/clay nanocomposites where there is no significant difference in thermal stability for the clay nanocomposites compared to pure polymer, when TGA is done under an inert atmosphere.

Table 3. Thermogravimetric analysis data for PA-6/graphite nanocomposites

| **Graphite** | **Graphite loading (%)** | **$T_{10\%}$ (°C)** | **$T_{max}$ (°C)** | **Char (%)** |
|---|---|---|---|---|
| Non-annealed samples | | | | |
| No filler | 0 | 406 ± 2 | 447 ± 5 | 4 ± 1 |
| VG | 1 | 419 ± 1 | 471 ± 3 | 2 ± 1 |
| | 3 | 415 ± 4 | 470 ± 5 | 5 ± 1 |
| | 5 | 410 ± 1 | 457 ± 0 | 7 ± 1 |
| EG | 1 | 409 ± 5 | 462 ± 5 | 3 ± 1 |
| | 3 | 415 ± 5 | 467 ± 3 | 4 ± 1 |
| | 5 | 412 ± 5 | 457 ± 3 | 6 ± 1 |
| GIC-220A | 1 | 411 ± 1 | 464 ± 2 | 4 ± 1 |
| | 3 | 415 ± 6 | 458 ± 4 | 2 ± 1 |
| | 5 | 396 ± 4 | 453 ± 7 | 6 ± 1 |
| GIC-220B | 1 | 417 ± 0 | 464 ± 4 | 2 ± 1 |
| | 3 | 404 ± 5 | 454 ± 5 | 5 ± 1 |
| | 5 | 396 ± 0 | 453 ± 1 | 6 ± 1 |
| GIC-220N | 1 | 416 ± 1 | 464 ± 4 | 4 ± 1 |
| | 3 | 376 ± 5 | 435 ± 1 | 5 ± 1 |
| | 5 | 395 ± 5 | 451 ± 6 | 6 ± 1 |
| GIC-160A | 1 | 386 ± 1 | 441 ± 4 | 3 ± 1 |
| | 3 | 398 ± 0 | 456 ± 1 | 6 ± 1 |
| | 5 | 399 ± 5 | 449 ± 5 | 7 ± 2 |
| Annealed samples | | | | |
| No filler | 0 | 412 ± 3 | 450 ± 4 | 2 ± 1 |
| VG | 1 | 410 ± 1 | 456 ± 3 | 3 ± 1 |
| | 3 | 415 ± 1 | 455 ± 4 | 9 ± 3 |
| | 5 | 418 ± 5 | 459 ± 5 | 8 ± 1 |
| EG | 1 | 411 ± 1 | 460 ± 0 | 4 ± 1 |
| | 3 | 404 ± 5 | 446 ± 5 | 7 ± 1 |
| | 5 | 416 ± 4 | 460 ± 3 | 6 ± 1 |
| GIC-220A | 1 | 415 ± 1 | 460 ± 0 | 5 ± 3 |
| | 3 | 396 ± 4 | 447 ± 5 | 5 ± 2 |

| | | | | |
|---|---|---|---|---|
| | 5 | 405 ± 6 | 466 ± 6 | 5 ± 1 |
| GIC-220B | 1 | 414 ± 3 | 457 ± 2 | 4 ± 1 |
| | 3 | 411 ± 3 | 455 ± 1 | 5 ± 1 |
| | 5 | 409 ± 5 | 457 ± 1 | 6 ± 1 |
| GIC-220N | 1 | 411 ± 4 | 465 ± 3 | 2 ± 1 |
| | 3 | 408 ± 6 | 461 ± 1 | 5 ± 1 |
| | 5 | 397 ± 2 | 452 ± 3 | 8 ± 1 |
| GIC-160A | 1 | 415 ± 1 | 456 ± 5 | 4 ± 1 |
| | 3 | 406 ± 2 | 460 ± 3 | 7 ± 1 |
| | 5 | 398 ± 1 | 458 ± 0 | 8 ± 1 |

For the expandable graphites with an onset of release of sulfuric acid at 220 °C (GIC-220A, GIC-220N, GIC-220B) the onset of degradation is enhanced for the 1% graphite systems, but for higher graphite loadings the presence of graphite appears to facilitate the onset of degradation, moving it to lower onset temperatures. Likewise, the maximum temperature of degradation for these nanocomposites is slightly increased at 1% graphite, but there is no significant difference at higher loadings. Thus high graphite loadings, 3% and 5%, apparently are detrimental to PA-6 stability while 1% graphite enhances thermal stability. This may be attributed to the presence of the acid within the graphite, release of which can facilitate the degradation of the PA-6. The lower thermal stability could be attributed to the release of acid degradation products at lower temperatures. This hypothesis is further supported by the behaviour of the composites based on the GIC-160A graphite (onset for release of sulfuric acid is 160 °C). For these systems a decrease in the onset and maximum temperatures of degradation is observed at all loading levels, most probably because sulfuric acid is released much more effectively for the processing temperature used (250 °C).

Table 3 also shows the TGA data for annealed PA-6/graphite nanocomposites; there is no significant difference in the data obtained by TGA for annealed and non-annealed PA-6/graphite nanocomposites. This behaviour strongly indicates that whatever mechanisms are in effect for the TGA behaviour of these systems, these processes take place during the melt blending of the composites and are not further affected by subsequent annealing.

### 3.2.3. Thermogravimetric analysis coupled with Fourier transform infrared spectroscopy (TGA/FT-IR)

The degradation of the PA-6/GIC nanocomposites was followed under isothermal conditions at 250 °C for 30 min; throughout this time period, the typical products for the expansion of the expandable graphites are observed; $SO_2$ (1400–1300 $cm^{-1}$ and 1150–1050 $cm^{-1}$), $CO_2$ (3700–3600 $cm^{-1}$ and 2400–2200 $cm^{-1}$), and water (4000–3600 $cm^{-1}$ and 1850–1350 $cm^{-1}$) (Fig. 10) [36].

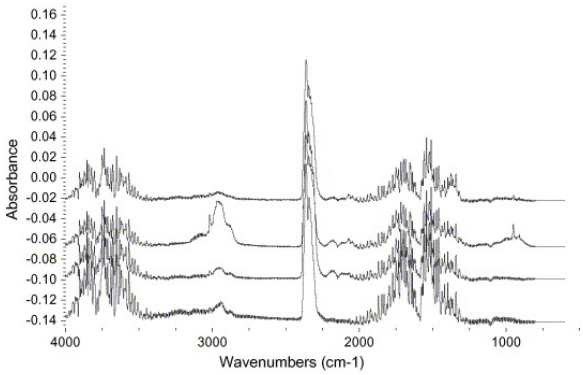


Fig. 10. TG/FT-IR of PA-6/GIC-160A nanocomposites; the temperatures from bottom to top are: 200 °C, 420 °C, 520 °C, and 600 °C.

Fig. 10 shows the infrared spectra of the gases evolved during a TGA/FT-IR experiment on a PA-6/GIC-160A nanocomposite from ambient temperature to 600 °C at 20 °C/min. Peaks due to $SO_2$, $CO_2$, and water are

observed throughout the run, indicating that reaction of sulfuric acid with the carbon occurs over the entire temperature range. Peaks in the aliphatic C–H stretching frequency range are observed beginning at 200 °C and peak about 500 °C; it is known that PA-6 will undergo depolymerisation in the presence of acid [51], [52] and these peaks are due to this depolymerisation reaction.

### 3.2.4. Mechanical properties

Fig. 11, Fig. 12 provide data on the tensile strength and elongation relative to that of virgin PA-6. It is clear that the presence of any graphite causes a deterioration in these properties but those systems which do not contain sulfuric acid, virgin and expanded graphite, causes the least amount of deterioration. This is not surprising considering the well-known acid instability of polyamides. The greatest deterioration in both tensile strength and elongation occur for GIC-160A, which has both an acid surface and loses its sulfuric acid at the lowest temperatures. It is surprising to note (Table 4) that Youngs modulus does not show a significant change for any of the graphite-containing systems, but there is a significant drop upon annealing. This is most likely due to the annealing process causing the release of some sulfuric acid with concomitant depolymerisation/degradation of the PA-6 and hence a decreased modulus.

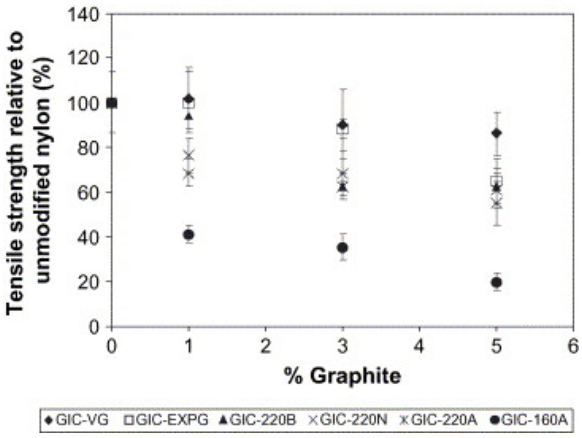


Fig. 11. Tensile strength of PA-6/graphite nanocomposites at 3% graphite relative to that of PA-6.

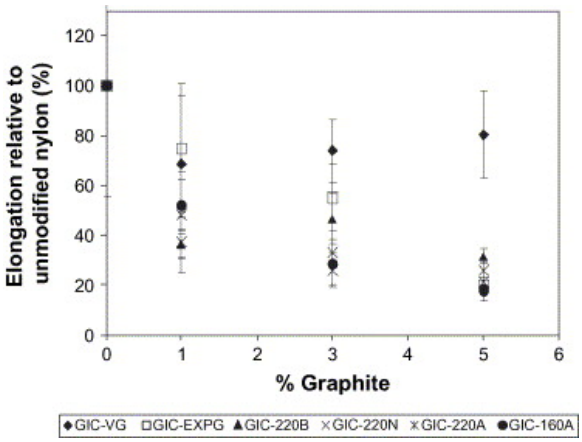


Fig. 12. Elongation of the PA-6/graphite nanocomposites at 3% graphite relative to the value of virgin PA-6.

Table 4. Youngs modulus for non-annealed and annealed samples

| Graphite | Graphite loading (%) | Youngs modulus (GPa) | |
|---|---|---|---|
| | | Non-annealed samples | Annealed samples |
| – | 0 | 1.4 ± 0.4 | 1.4 ± 0.4 |
| VG | 1 | 1.8 ± 0.5 | 1.2 ± 0.3 |
| | 3 | 1.3 ± 0.2 | 0.67 ± 0.12 |
| | 5 | 1.2 ± 0.2 | 1.1 ± 0.1 |

| | | | |
|---|---|---|---|
| EG | 1 | 1.3 ± 0.2 | 0.95 ± 0.10 |
| | 3 | 1.6 ± 0.5 | 0.96 ± 0.16 |
| | 5 | 1.6 ± 0.3 | 0.87 ± 0.21 |
| GIC-220B | 1 | 1.2 ± 0.1 | 1.2 ± 0.1 |
| | 3 | 1.7 ± 0.34 | 0.67 ± 0.15 |
| | 5 | 1.0 ± 0.2 | 0.57 ± 0.01 |
| GIC-220N | 1 | 1.3 ± 0.2 | 0.49 ± 0.11 |
| | 3 | 1.4 ± 0.3 | 0.79 ± 0.13 |
| | 5 | 1.1 ± 0.3 | 0.79 ± 0.13 |
| GIC-220A | 1 | 1.3 ± 0.2 | 0.56 ± 0.09 |
| | 3 | 1.3 ± 0.3 | 0.67 ± 0.15 |
| | 5 | 1.1 ± 0.0 | 0.77 ± 0.15 |
| GIC-160A | 1 | 1.4 ± 0.2 | 0.49 ± 0.07 |
| | 3 | 1.4 ± 0.3 | 0.55 ± 0.10 |
| | 5 | 1.2 ± 0.3 | 0.31 ± 0.07 |

Some of these graphite-filled nanocomposites have a nanocomposite structure which is similar to that of the PA-6/montmorillonite system, this difference in tensile behaviour should be attributed to the synergy of two factors:

a) The high density of hydrogen bonding between the PA-6 and the montmorillonite silicate layers, which is largely absent here. Extensive hydrogen bonding between the polymer and the filler can strongly reinforce the composites since it facilitates a much more effective stress-transfer from the matrix to the fillers [18]. Moreover, this same hydrogen bonding also promotes the γ crystal phase in clay-filled PA-6, which is known to have superior tensile properties compared to the α crystal phase of the neat (unfilled) PA-6 [24], [25].
b) The lower modulus of the graphite layers compared to that of the montmorillonite silicate layer.

### 3.2.5. Dynamic mechanical analysis (DMA)

Dynamic mechanical analysis indicates that storage modulus (*E*') for PA-6/graphite nanocomposites is lower than that of neat PA-6 as shown in Fig. 13. Assuming that the peak temperature of loss moduli is indicative of the glass transition temperature ($T_g$), $T_g$ of PA-6 decreased and the peak broadened by the addition of graphite (Fig. 14). These results are in good agreement with the tensile behaviour discussed above, however, a detailed discussion on the origin of these phenomena needs further careful investigation.

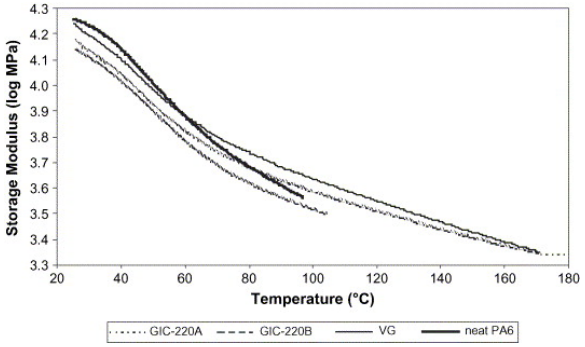


Fig. 13. Storage modulus of PA-6/graphite nanocomposites at 3% graphite.

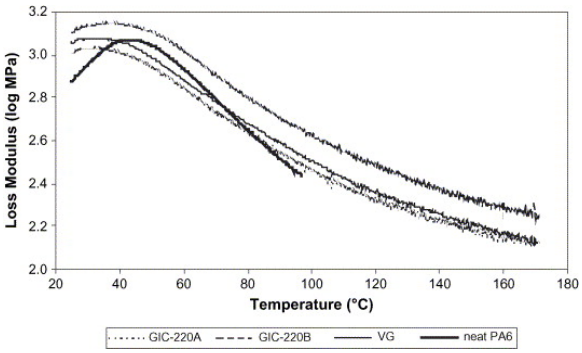

Fig. 14. Loss modulus for PA-6/graphite nanocomposites at 3% graphite.

## 4. Conclusions

Polyamide-6 (PA-6)/graphite nanocomposites were prepared by melt blending. Good nanometre-scale dispersion of graphites was achieved for specific treatments of graphite; based on X-ray diffraction analyses, TEM observations, and cone calorimetry analyses, PA-6/expandable-graphite nanocomposites showed an intercalated/exfoliated nanocomposite structure. Thermogravimetric analysis (TGA) under nitrogen showed little change in thermal stability, in agreement with the observations from PA-6/clay nanocomposites. Cone calorimetric data showed a very significant reduction in peak heat release rate, even larger than what has been observed in PA-6/clay systems, but only for those graphites which can release sulfuric acid degradation products during melt blending. The tensile moduli of PA-6 were slightly improved by the graphite addition, although this improvement took place at the expense of elongation at break and strength.

When compared to PA-6/montmorillonite clay nanocomposites of similar composite structures – i.e. comparable filler dispersions –, the PA-6/graphite nanocomposites herein show superior flame retardant properties, but not as good thermo-mechanical properties as the PA-6/clay equivalents. This behaviour strongly indicates that the composite structure and filler chemistry affect the flame retardancy in a similar manner in these two classes of nanocomposites, whereas the silicate (clay) fillers are much more beneficial also for the mechanical properties. This latter fact is herein attributed to the strong hydrogen bonding between PA-6 and silicate clays.

## Acknowledgements

This work was performed under the sponsorship of the US Department of Commence, National Institute of Standards and Technology, Grant Number 70NANB6D0119. The authors thank Ms. M. Hazen (Penn State LSC) for aiding with the TEM studies. HN acknowledges support from Sumitomo Chemical, Japan, and EM from the "Virginia S. and Philip L. Walker Jr." Endowed Faculty Fellowship and the AFOSR.

**References**

[1] A. Usuki, Y. Kojima, A. Okada, Y. Fukushima, T. Kurauchi, O. Kamigaito. *J Mater Res, 8* (1993), pp. 1179-1184
[2] M. Alexandre, P. Dubois. *Mater Sci Eng R,* 28 (2000), pp. 1-63
[3] P.C. LeBaron, Z. Wang, T.J. Pinnavaia. *Appl Clay Sci*, 15 (1999), pp. 11-29
[4] E.P. Giannelis, R.K. Krishnamoorti, E. Manias. *Adv Polym Sci*, 138 (1998), pp. 107-143
[5] R. Krishnamoorti, R.A. Vaia, E.P. Giannelis. *Chem Mater*, 8 (1996), pp. 1728-1734
[6] J.W. Cho, D.R. Paul. *Polymer*, 42 (2001), pp. 1083-1094
[7] J. Zhu, F.M. Uhl, A.B. Morgan, C.A. Wilkie. *Chem Mat,* 13 (2001), pp. 4649-4654
[8] J. Zhu, A.B. Morgan, F.J. Lamelas, C.A. Wilkie. *Chem Mat,* 13 (2001), pp. 3774-3780
[9] D. Wang, D. Parlow, Q. Yao, C.A. Wilkie. *J Vinyl Add Tech*, 77 (2001), pp. 203-213
[10] J. Zhu, F. Uhl, C.A. Wilkie. G.L. Nelson, C.A. Wilkie (Eds.), *Fire and polymers materials and solutions for hazard prevention*, Oxford University Press (2001), pp. 24-33

[11] A.B. Morgan, T. Kashiwagi, R.H. Harris, J.R. Campbell, K. Shibayama, K. Iwasa, *et al.*. G.L. Nelson, C.A. Wilkie (Eds.), *Fire and polymers materials and solutions for hazard prevention*, Oxford University Press (2001), pp. 9-23
[12] J. Zhu, C.A. Wilkie. *Polym Int*, 49 (2000), pp. 1158-1163
[13] X. Fu, S. Qutubuddin. *Polymer*, 42 (2001), pp. 807-813
[14] J.W. Gilman, C.L. Jackson, A.B. Morgan, R. Harris, E. Manias, E.P. Giannelis, *et al.. Chem Mat*, 12 (2000), pp. 1866-1873
[15] J.W. Gilman, T. Kashiwagi, S. Lomakin. M. LeBras, G. Camino, S. Bourbigot, R. Delobel (Eds.), *Fire retardancy of polymers: the use of intumescence*, Royal Society of Chemistry, London (1998), pp. 201-221
[16] L. Liu, Z. Qi, X. Zhu. *J Appl Polym Sci*, 71 (1999), pp. 1133-1138
[17] Y.X. Pan, Z.Z. Yu, Y.C. Ou, G.H. Hu. *J Polym Sci Part B Polym Phys*, 38 (2000), pp. 1626-1633
[18] E. Manias, A. Touny, L. Wu, K. Strawhecker, B. Lu, T.C. Chung. *Chem Mater*, 13 (2000), pp. 3516-3523
[19] K.E. Strawhecker, E. Manias. *Chem Mat*, 12 (2000), pp. 2943-2949
[20] R.A. Vaia, S. Vasudevan, W. Krawiec, L.G. Scanlon, E.P. Giannelis. *Adv Mater*, 7 (1995), pp. 154-156
[21] (a) A.C. Balazs, C. Singh, E. Zhulina, Y. Lyatskaya. *Acc Chem Res*, 32 (1999), pp. 651-657. (b) A.C. Balazs, C. Singh, E. Zhulina, Y. Lyatskaya. *Macromolecules*, 31 (1998), pp. 8370-8381
[22] R.A. Vaia, E.P. Giannelis. *Macromolecules*, 30 (1997), pp. 7990-7999
[23] Y. Kojima, A. Usuki, M. Kawasumi, A. Okada, T. Kurauchi, O. Kamigaito. *J Polym Sci Part A Polym Chem*, 31 (1993), pp. 1755-1758
[24] D.M. Lincoln, R.A. Vaia, R. Krishnamoorti. *Macromolecules*, 37 (2004), pp. 4554-4561
[25] D.M. Lincoln, R.A. Vaia, Z.G. Wang, B.S. Hsiao, R. Krishnamoorti. *Polymer*, 42 (2001), pp. 9975-9985
[26] J.M. Lalancette, R. Roussel. *Can J Chem*, 54 (1976), pp. 2110-2115
[27] J.M. Lalancette, R. Rollin, P. Dumas. *Can J Chem*, 50 (1972), pp. 3058-3062
[28] G.R. Hennig. *Prog Inorg Chem*, 1 (1959), pp. 125-133
[29] W. Rudorff. *Adv Inorg Radiochem*, 1 (1959), pp. 223-266
[30] H. Selig, L.B. Ebert. *Adv Inorg Radiochem*, 23 (1980), pp. 289-327
[31] H. Shioyama. *Carbon*, 35 (1997), pp. 1664-1665
[32] H. Shioyama. *Synth Met*, 114 (2000), pp. 1-15
[33] H. Shioyama, K. Tatsumi, N. Iwashita, K. Fujita, Y. Sawada. *Synth Met,* 96 (1998), pp. 229-233
[34] H. Shioyama. *Mol Cryst Liq Cryst*, 340 (2000), pp. 101-106
[35] F.M. Uhl, C.A. Wilkie. *Polym Degrad Stab*, 76 (2002), pp. 111-122
[36] G. Camino, S. Duquesne, R. Delobel, B. Eling, C. Lindsay, T. Roles. G.L. Nelson, C.A. Wilkie (Eds.), *Fire and polymers materials and solutions for hazard prevention*, Oxford University Press (2001), pp. 90-109
[37] F. Kang, T.Y. Zhang, Y. Leng. *Carbon*, 35 (1997), pp. 1167-1173
[38] G.-H. Chen, D.-J. Wu, W.-G. Weng, B. He, W.-L. Yan. *Polym Int*, 50 (2001), pp. 980-985
[39] W.G. Weng, G.H. Chen, D.J. Wu. *Polymer*, 44 (2003), pp. 8119-8132
[40] G.H. Chen, W.G. Weng, D.J. Wu, C.L. Wu. *J Polym Sci Part B Polym Phys*, 42 (2004), pp. 155-167
[41] J.W. Gilman, T. Kashiwagi, M. Nyden, J.E.T. Brown, C.L. Jackson, S. Lomakin, *et al.* S. Al-Maliaka, A. Golovoy, C.A. Wilkie (Eds.), *Chemistry and technology of polymer additives*, Blackwell Scientific, London (1998), pp. 249-265
[42] N. Vasanthan, D.R. Salem. *J Polym Sci Part B Polym Phys*, 39 (2001), pp. 536-547
[43] Y. Kojima, T. Matsuoka, H. Takahashi, T. Kurauchi. *J Appl Polym Sci*, 51 (1994), pp. 683-687
[44] A.L. Simal, A.E. Martin. *J Appl Polym Sci*, 68 (1998), pp. 441-452
[45] A.L. Simal, A.E. Martin. *J Appl Polym Sci* (1998), pp. 453-474
[46] J.W. Gilman, T. Kashiwagi, E.P. Gianellis, E. Manias, S. Lomakin, J.D. Lichtenhan, *et al.*. M. Le Bras, G. Camino, S. Bourbigot, R. Delobel (Eds.), *Fire retardancy: the use of intumescence*, Royal Society of Chemistry, Cambridge (1998), pp. 203-221
[47] S. Su, D.D. Jiang, C.A. Wilkie. *J Vinyl Add Tech*, 10 (2004), pp. 44-51
[48] J.W. Gilman, T. Kashiwagi. T.J. Pinnavaia, G.W. Beall (Eds.), *Polymer–clay nanocomposites*, John Wiley & Sons(2001), pp. 193-206

[49] J. Zhu, F.M. Uhl, A.B. Morgan, C.A. Wilkie. *Chem Mater*, 13 (2001), pp. 4649-4654
[50] Jaromi, S, Gabrie¨lse, W, Braam, A. *Proceedings on additives* 2002. Clearwater Beach, FL; March 2002.
[51] T. Konomi, H. Tani. *J Polym Sci Part A-1*, 8 (1970), pp. 1261-1268
[52] L.J. Mathias, R.A. Vaidya, J.B. Canterberry. *J Chem Educ*, 61 (1984), pp. 805-807